Colloidal diamond

Mingxin He, Johnathon P Gales, Étienne Ducrot, Zhe Gong, Gi-Ra Yi, Stefano Sacanna, David J Pine

Colloidal diamond

Mingxin He[1,2], Johnathon P. Gales[2], Étienne Ducrot[2,3], Zhe Gong[4], Gi-Ra Yi[5], Stefano Sacanna[4] and David J. Pine[1,2]

[1]Department of Chemical and Biomolecular Engineering, New York University, Brooklyn, NY, USA.
[2]Department of Physics, Center for Soft Matter Research, New York University, New York, NY, USA.
[3]University of Bordeaux, CNRS, Centre de Recherche Paul Pascal, Pessac, France.
[4]Department of Chemistry, Molecular Design Institute, New York University, New York, NY, USA.
[5]School of Chemical Engineering, Sungkyunkwan University, Suwon, South Korea.

Self-assembling colloidal particles in the cubic diamond crystal structure could potentially be used to make materials with a photonic bandgap[1–3]. Such materials are beneficial because they suppress spontaneous emission of light[1] and are valued for their applications as optical waveguides, filters and laser resonators[4], for improving light-harvesting technologies[5–7] and for other applications[4,8]. Cubic diamond is preferred for these applications over more easily self-assembled structures, such as face-centred-cubic structures[9,10], because diamond has a much wider bandgap and is less sensitive to imperfections[11,12]. In addition, the bandgap in diamond crystals appears at a refractive index contrast of about 2, which means that a photonic bandgap could be achieved using known materials at optical frequencies; this does not seem to be possible for face-centred-cubic crystals[3,13]. However, self-assembly of colloidal diamond is challenging. Because particles in a diamond lattice are tetrahedrally coordinated, one approach has been to self-assemble spherical particles with tetrahedral sticky patches[14–16]. But this approach lacks a mechanism to ensure that the patchy spheres select the staggered orientation of tetrahedral bonds on nearest-neighbour particles, which is required for cubic diamond[15,17]. Here we show that by using partially compressed tetrahedral clusters with retracted sticky patches, colloidal cubic diamond can be self-assembled using patch–patch adhesion in combination with a steric interlock mechanism that selects the required staggered bond orientation. Photonic bandstructure calculations reveal that the resulting lattices (direct and inverse) have promising optical properties, including a wide and complete photonic bandgap. The colloidal particles in the self-assembled cubic diamond structure are highly constrained and mechanically stable, which makes it possible to dry the suspension and retain the diamond structure. This makes these structures suitable templates for forming high-dielectric-contrast photonic crystals with cubic diamond symmetry.

The superior optical properties of cubic diamond compared to other self-assembled structures has led to investigations of the possibility of self-assembling a diamond lattice from colloidal spheres[14,16,18,19]. However, the diamond lattice poses a challenge for colloidal self-assembly. The spheres in a diamond lattice are tetrahedrally coordinated (Fig. 1a), which means that they have two fewer constraints than the six required for mechanical stability and a maximum packing fraction of $\pi\ 3/16 \approx 0.34$. Unlike face-centred-cubic colloidal crystals[9], in which the spheres have 12 nearest neighbours and a maximum packing fraction of $\pi/\ 18 \approx 0.74$, diamond crystals cannot be stabilized by entropy alone.

One way to address this challenge is to self-assemble a superlattice of two or more colloidal species, with one of the sublattices being diamond[19–22]. This solves the low-packing-density problem by backfilling the voids with a temporary lattice that is ultimately removed, but doing so is delicate and has yet to be demonstrated. Another approach is to build a three-dimensional DNA scaffold and tether small gold nanoparticles within the scaffold[23], but the length scales are too small and the particles are disconnected, precluding the formation of photonic bandgaps. Yet another approach is to use faceted particles with attractive interactions, which has yielded some surprising results, such as colloidal clathrate[24]. This approach is related to an earlier one, suggested on the basis of simulations[25], which involves triangular di-patches on spheres and can produce colloidal clathrate or diamond, depending on the relative orientations of the di-patches. In other simulations, certain truncated tetrahedra are predicted to have diamond phases[26], but it is not clear whether they could serve as templates for photonic crystals.

In devising any method to make diamond photonic crystals, it is important to distinguish between cubic and hexagonal diamond. Cubic diamond has a photonic bandgap; hexagonal diamond does not. An important difference between cubic and hexagonal diamond is the way each particle is connected to its four nearest neighbours[15]. For cubic diamond, all four nearest neighbours are connected in the staggered conformation (Fig. 1b). For hexagonal diamond, only three of the four nearest neighbours are connected in the staggered conformation; the fourth is connected in the eclipsed conformation (Fig. 1b)[15]. In atomic crystals, the staggered conformation is preferred because the *sp*3 bonding electrons between next-nearest-neighbour bonds are further away from each other than they are in the eclipsed conformation, minimizing the Coulomb energy. In a colloidal system, it is difficult to achieve both an attractive interaction that binds patches together and, simultaneously, a long-range interaction that produces either the staggered or eclipsed conformation. Therefore, for spherical patchy colloids, no conformation—staggered, eclipsed or anything in between—is energetically favoured (Fig. 1c, left, Supplementary Video 1).

Here we show that the rotational information needed to select the staggered conformation can be written into the shape of the particles. The idea of using shaped colloidal clusters to direct colloidal self-assembly has been well investigated[18, 20, 27–31]. Figure 1c illustrates our particle design strategy. Each particle consists of four tetrahedrally coordinated, partially overlapping spherical lobes, shown in purple or white. At the centre of each of the four triangular faces is a DNA-coated patch, shown in light blue. The DNA on the patches is designed with self-complementary sticky ends so that patches on different particles are attractive below the melting temperature *T*m of DNA patch. The radial extent of the patches is retracted from the plane formed by the convex hull of the spherical lobes. This means that the DNA on the patches of different particles can reach each other and bind only if the lobes on different particles are oriented in the staggered conformation, as shown in Fig. 1c. Below, we show with simulations and experiments that this is sufficient to stabilize the cubic diamond structure. Figure 1d, e and Supplementary Video 2 show the diamond unit cell formed by these particles.

Particle synthesis

The synthesis of our patchy compressed clusters builds on a colloidal fusion protocol reported recently[32]. In this protocol (Fig. 2a), solid non-crosslinked polystyrene particles are mixed with smaller droplets of a polymerizable oil, 3-trimethoxysilyl propyl methacrylate (TPM). When the ratio of the diameters of the solid particles and liquid droplets is near $\alpha = 1 + 2 \approx 2.41$, the stochastic aggregation of solid particles onto the smaller liquid droplets results in tetrahedral clusters—four solid particles bound to a liquid droplet—with nearly 100% yield[32,33] (Methods). Density gradient centrifugation removes the small number of non-tetrahedral clusters. In the end, fewer than 1 in 1,000 particles are not tetrahedra.

The next step is the controlled deformation of the polystyrene spheres by the addition of a plasticizer to the suspension; we use tetrahydrofuran (THF). The deformation of the spheres extrudes the liquid core of the clusters such that the core protrudes out of the interstices between each set of three polystyrene particles that form the four faces of the clusters. This is performed at room temperature, which allows us to finely tune the degree to which the polystyrene spheres are compressed and the liquid core is extruded (Fig. 2b). To characterize the geometry of the partially deformed clusters, two parameters are introduced: the compression ratio of the polystyrene spheres and the size ratio of the patches to the spheres (Fig. 2c, d). The compression and size ratios can be finely tuned by varying the concentration of plasticizer (THF) and the types of surfactant used (Extended Data Fig. 1). A compression ratio of 0 means that the four original polystyrene particles have coalesced into a single sphere; a compression ratio of 1 means that the clusters are not compressed at all.

The clusters depicted in Fig. 2 have a compression ratio of 0.78, which is typical for our experiments.

Although the size and compression ratios are closely linked, they can be independently adjusted to some degree. By using different surfactants, which control the wetting angle between a TPM droplet and its polystyrene cluster, the size ratio can be changed. We find that using sodium dodecyl sulfate (SDS) gives the right amount of wetting[34] (Methods). To fix the geometry of the patchy cluster, the plasticizer is evaporated to harden the polystyrene cluster and the liquid cores are solidified by free radical polymerization. Before clustering, the TPM oil is functionalized with epoxy groups by introducing (3-glycidyloxypropyl) trimethoxysilane. After deformation and polymerization, these epoxy groups are converted to azide groups, which can further react with dibenzocyclooctyne (DBCO)-functionalized DNA by strain-promoted azide-alkyne cycloaddition chemistry[35].

Because only the TPM patches have these surface functional groups, we can selectively functionalize the TPM patches with single-stranded DNA and leave the surfaces of the polystyrene spheres nearly bare (Extended Data Fig. 2). Although the preparation of these tetrahedral patchy colloidal clusters is complex, the experimental design is simple: it uses a single type of particle, with patches functionalized with a single type of DNA. Moreover, the self-assembly is robust, crystallization is relatively fast, and cubic diamond is the only product.

Particle design and crystallization

To guide the design of our particles and verify the conditions under which they might crystallize into cubic diamond, we performed simulations using the HOOMD-blue simulation package[36,37] (Methods). The phase diagram determined by the simulations is shown in Extended Data Fig. 3. We also performed numerical calculations of the photonic band structures of the resultant direct and inverse lattices using the MIT Photonic Bands software[38] (see 'Calculation of photonic bandgap'). The outcomes of these two sets of calculations led us to explore particles with compression ratios between 0.63 and 0.78, and size ratios near 1.2. The size of the primary polystyrene particles from which the compressed tetrahedral clusters are made was chosen to be 1.0 μm, as this leads to a photonic bandgap centred at the technologically interesting wavelength of 1.5 μm, at which most optical communications networks work.

Starting from 1.0-μm primary polystyrene particles, the resulting compressed clusters are slightly smaller than 2.0 μm across, resulting in substantial sedimentation, with a gravitational height of 2 μm in water. As shown in Extended Data Fig. 4, the particles bind, interlock and form small crystals after annealing overnight. To grow bigger crystals, the particles are nearly density-matched by suspending them in a mixture of H2O and D2O (with PBS buffer), which

increases the gravitational height from about 2 μm to 20 μm. The suspension is loaded into a glass capillary and sealed, with typical dimensions of 100 μm × 2 mm × 50 mm. The capillary is tilted at 20° along the 2-mm dimension to provide an exponential atmosphere of particles and promote slow growth and annealing. A temperature gradient of about 1 °C, which spans the melting temperature of the DNA-coated patches, is applied along the long, 50-mm length of the capillary. The compressed clusters crystallize overnight, with typical crystal sizes of 40 μm, and some extending to 100 μm or more (Fig. 3a).

To examine the crystal structure, the TPM cores are fluorescently labelled before polymerization when the clusters are prepared. Figure 3a–c shows images taken in the horizontal plane with a fluorescent microscope. Figure 3a, b reveals the honeycomb pattern characteristic of the 111 plane of diamond; the polystyrene lobes of the particles are not visible as they are not dyed. Figure 3c shows a crystal in which the 110 plane of cubic diamond can be seen. Whereas the 111 plane (Fig. 3a, b) appears in both the cubic and hexagonal versions of diamond, the 110 plane (Fig. 3c) is unique to the cubic diamond lattice.

To further examine the structure of the self-assembled crystals, the hybridized DNA bonds that link the patches of neighbouring particles are permanently crosslinked via exposure to ultraviolet radiation in the presence of 8-methoxypsoralen (Methods)[39]. This allows the samples to be removed from the capillary and dried without disturbing their structure. To facilitate optical measurements in three dimensions, a sample is immersed in index-matching oil and viewed with a confocal microscope. The confocal *z* stacks reveal an ABC stacking of the 111 honeycomb planes, which confirms that the crystals are cubic diamond (Supplementary Videos 3, 4) and not hexagonal diamond, which has an AB stacking of the 111 planes. The confocal images show that the crystals are typically 10 or more layers thick, isotropic and fully three dimensional.

We also view the psoralen-crosslinked dried crystals with a scanning electron microscope. Figure 3f confirms that the crystal is well preserved after drying. Figure 3g shows a side view of the dried crystal and reveals that the thickness of the diamond crystal is about 10 layers.

Calculation of photonic bandgap

It is well established that diamond lattices of spheres exhibit a photonic bandgap. But the question of whether diamond lattices assembled from tetrahedral patchy clusters could also exhibit photonic bandgaps has not previously been considered. To address this question, we performed a series of photonic band structure calculations using the MIT Photonic Bands software38.

We consider the direct and inverse lattices. The direct lattice is a cubic diamond lattice made of tetrahedral clusters like the ones we used, but with a higher refractive index. The inverse lattice is obtained by backfilling the interstices of the direct lattice with a high-index dielectric material, after which the original tetrahedral clusters are removed, leaving only air behind. The inset in Fig. 4 shows the unit cell of the inverse lattice (see also Extended Data Fig. 5a, Supplementary Video 5). We choose refractive indices of 2.6 and 3.4, corresponding to TiO2 and silicon, respectively, as these materials have high refractive indices in the visible and near-infrared, exhibit very little absorption of light in their respective frequency ranges and can be fabricated experimentally.

These calculations reveal that the direct and inverse (Extended Data Fig. 5c) cluster diamond lattices both have complete photonic bandgaps between the second and third bands, consistent with the photonic properties of conventional diamond lattices of spheres.

Figure 4 shows how the relative width of the bandgap changes as the compression ratio is varied from 0 (a diamond lattice of non-overlapping spheres) to 1 (a diamond lattice of uncompressed clusters), for refractive indices of 2.6 (TiO2) and 3.4 (silicon). These calculations reveal that the use of compressed clusters ($0.1 \leq d\text{cc}/(2a) \leq 0.8$) opens up a bandgap for the inverse lattice, whereas no bandgap appears for non-overlapping spheres ($d\text{cc}/(2a) = 0$). The widest bandgap is achieved slightly below or above a compression ratio of 0.6, depending on the value of the refractive index. This is very near the compression ratios that we have already found result in crystallization experimentally: $0.63 \leq d\text{cc}/(2a) \leq 0.78$ (Fig. 4, light blue). By contrast, using compressed clusters improves the bandgap only slightly for the direct lattice, with the widest bandgap occurring near $d\text{cc}/(2a) = 0.15$ and diminishing to 0 when $d\text{cc}/(2a) = 0.6$. In all of these calculations, the size ratio is fixed so that the patches touch precisely when the spherical lobes touch for neighbouring particles in the staggered conformation. Variations in the size ratio have very little effect on the bandgap.

On the basis of previous numerical studies of the photonic bandgap of diamond crystals11, we expect the bandgap of the cubic diamond crystals described here to be robust with respect to disorder and various kinds of defects. Moreover, the crystals grown experimentally show good order, aided by the steric interlocking of clusters. In the geometric limit of ideal packing, each of the four faces of a colloidal cluster has six points of contact with its neighbour—seven including the sticky patch. This very large number of contact points per particle (28) helps to ensure orientational order.

Next steps

The cubic diamond colloidal crystals described here are made from polystyrene and TPM, which have refractive indices of 1.6 and 1.4, respectively, too low to open up a photonic bandgap. Materials with refractive indices larger than 2 are needed to realize a photonic bandgap (Extended Data Fig. 5d). The simplest strategy to achieve this is to use our colloidal crystals as templates to make an inverse diamond structure by backfilling the interstices with a high-refractive-index material and then removing the colloidal template. Sol–gel chemistry[40–42] or atomic layer deposition[43,44] can be used to backfill a colloidal crystal with TiO2, which has a refractive index of around 2.6 in the visible and near-infrared. Similarly, chemical vapour deposition[10,45] can be used to backfill a colloidal crystal with silicon, which has a refractive index of 3.4 in the near-infrared. Because chemical vapour deposition takes place at temperatures above the glass transition temperature of polystyrene of 105 °C, a low-temperature process such as atomic layer deposition should be used to first coat the colloidal crystal with a protective oxide layer, after which the template can be coated with silicon using chemical vapour deposition[45]. The protective oxide layer can be left in place or removed (along with any remnant of the colloidal template) after the backfilling with silicon is complete. Extended Data Fig. 5b shows a rendering of the inverse lattice with the oxide layer removed. Removing the protective oxide layer increases the bandgap substantially. The grey line in Fig. 4 shows the bandgap obtained using a protective layer with a thickness of 0.1*a*, followed by backfilling with silicon. For a compression ratio of 0.65, the bandgap increases from 14% to 22%. Even greater increases can be achieved using thicker protective oxide layers.

To realize the optical properties of photonic bandgaps, crystals that are ten or more unit cells thick are desirable. We have grown colloidal diamond crystals with lateral dimensions of up to 80 μm (about 30 unit cells) and thicknesses of up to 40 μm (about 15 unit cells). Although this is sufficiently large to investigate the photonic bandgap properties of these materials, crystals of larger lateral extent (several millimetres or more in size) would be more suitable for optical waveguides, lasers and other optical applications. There are well established methods to grow large colloidal crystals, such as epitaxial growth from a templated surface[46].

The inverse structure of the crystals reported here would have a photonic bandgap centred in the infrared, around a wavelength of 1.5 μm. As the photonic band structure scales with the crystal lattice constant, the particle size would need to be reduced by a factor of two to realize a bandgap in the visible range. The smaller size would make following the crystallization using an optical microscope more difficult, making experiments more challenging. The particles would probably be more polydisperse, but it should be feasible.

Our approach combines directional interactions with a steric interlock mechanism that orients the attractive patches in the desired staggered conformation. We note that particle shape alone

is insufficient to form diamond; removing the attractive interaction between patches results in amorphous structures. Our work suggests that, similarly to our DNA hybridization approach, any attractive interaction between patches—such as depletion[47], hydrophobic[48] or critical Casimir interactions[49]— should yield cubic diamond colloidal crystals.

1. Yablonovitch, E. Inhibited spontaneous emission in solid-state physics and electronics. *Phys. Rev. Lett*. 58, 2059–2062 (1987).

2. John, S. Strong localization of photons in certain disordered dielectric superlattices. *Phys. Rev. Lett*. 58, 2486–2489 (1987).

3. Ho, K. M., Chan, C. T. & Soukoulis, C. M. Existence of a photonic gap in periodic dielectric structures. *Phys. Rev. Lett*. 65, 3152–3155 (1990).

4. Joannopoulos, J. D., Johnson, S. G., Winn, J. N. & Meade, R. D. *Photonic Crystals: Molding the Flow of Light* 2nd edn (Princeton Univ. Press, 2008).

5. Halaoui, L. I., Abrams, N. M. & Mallouk, T. E. Increasing the conversion efficiency of dye-sensitized TiO2 photoelectrochemical cells by coupling to photonic crystals. *J. Phys. Chem. B* 109, 6334–6342 (2005).

6. Bermel, P., Luo, C., Zeng, L., Kimerling, L. C. & Joannopoulos, J. D. Improving thin-film crystalline silicon solar cell efficiencies with photonic crystals. *Opt. Express* 15, 16986–17000 (2007).

7. Zhang, Z., Zhang, L., Hedhili, M. N., Zhang, H. & Wang, P. Plasmonic gold nanocrystals coupled with photonic crystal seamlessly on TiO2 nanotube photoelectrodes for efficient visible light photoelectrochemical water splitting. *Nano Lett*. 13, 14–20 (2013).

8. Yanik, M. F., Fan, S., Soljacić, M. & Joannopoulos, J. D. All-optical transistor action with bistable switching in a photonic crystal cross-waveguide geometry. *Opt. Lett*. 28, 2506–2508 (2003).

9. Pusey, P. N. & van Megen, W. Phase behaviour of concentrated suspensions of nearly hard colloidal spheres. *Nature* 320, 340–342 (1986).

10. Vlasov, Y. A., Bo, X. Z., Sturm, J. C. & Norris, D. J. On-chip natural assembly of silicon photonic bandgap crystals. *Nature* 414, 289–293 (2001).

11. Sigalas, M. M., Soukoulis, C. M., Chan, C. T., Biswas, R. & Ho, K. M. Effect of disorder on photonic band gaps. *Phys. Rev. B* 59, 12767–12770 (1999).

12. Li, Z.-Y. & Zhang, Z.-Q. Fragility of photonic band gaps in inverse-opal photonic crystals. *Phys. Rev. B* 62, 1516–1519 (2000).

13. Busch, K. & John, S. Photonic band gap formation in certain self-organizing systems. *Phys. Rev. E* 58, 3896–3908 (1998).

14. Zhang, Z., Keys, A. S., Chen, T. & Glotzer, S. C. Self-assembly of patchy particles into diamond structures through molecular mimicry. *Langmuir* 21, 11547–11551 (2005).

15. Romano, F., Sanz, E. & Sciortino, F. Crystallization of tetrahedral patchy particles in silico. *J. Chem. Phys*. 134, 174502 (2011).

16. Wang, Y. et al. Colloids with valence and specific directional bonding. *Nature* 491, 51–55 (2012).

17. Noya, E. G., Zubieta, I., Pine, D. J. & Sciortino, F. Assembly of clathrates from tetrahedral patchy colloids with narrow patches. *J. Chem. Phys*. 151, 094502 (2019).

18. Manoharan, V. N., Elsesser, M. T. & Pine, D. J. Dense packing and symmetry in small clusters of microspheres. *Science* 301, 483–487 (2003).

19. Hynninen, A.-P., Thijssen, J. H. J., Vermolen, E. C. M., Dijkstra, M. & van Blaaderen, A. Self-assembly route for photonic crystals with a bandgap in the visible region. *Nat. Mater*. 6, 202–205 (2007).

20. Zanjani, M. B., Jenkins, I. C., Crocker, J. C. & Sinno, T. Colloidal cluster assembly into ordered superstructures via engineered directional binding. *ACS Nano* 10, 11280–11289 (2016).

21. Wang, Y., Jenkins, I. C., McGinley, J. T., Sinno, T. & Crocker, J. C. Colloidal crystals with diamond symmetry at optical lengthscales. *Nat. Commun*. 8, 14173 (2017).

22. Ducrot, É., He, M., Yi, G. R. & Pine, D. J. Colloidal alloys with preassembled clusters and spheres. *Nat. Mater*. 16, 652–657 (2017).

23. Liu, W. et al. Diamond family of nanoparticle superlattices. *Science* 351, 582–586 (2016).

24. Lin, H. et al. Clathrate colloidal crystals. *Science* 355, 931–935 (2017).

25. Romano, F. & Sciortino, F. Patterning symmetry in the rational design of colloidal crystals. *Nat. Commun*. 3, 975 (2012).

26. Damasceno, P. F., Engel, M. & Glotzer, S. C. Crystalline assemblies and densest packings of a family of truncated tetrahedra and the role of directional entropic forces. *ACS Nano* 6, 609–614 (2012).

27. Perro, A. et al. A chemical synthetic route towards "colloidal molecules". *Angew. Chem. Int. Ed*. 48, 361–365 (2009).

28. Sacanna, S. & Pine, D. J. Shape-anisotropic colloids: building blocks for complex assemblies. *Curr. Opin. Colloid Interface Sci*. 16, 96–105 (2011).

29. Grünwald, M. & Geissler, P. L. Patterns without patches: hierarchical self-assembly of complex structures from simple building blocks. *ACS Nano* 8, 5891–5897 (2014).

30. McGinley, J. T., Wang, Y., Jenkins, I. C., Sinno, T. & Crocker, J. C. Crystal-templated colloidal clusters exhibit directional DNA interactions. *ACS Nano* 9, 10817–10825 (2015).

31. Ducrot, É., Gales, J., Yi, G.-R. & Pine, D. J. Pyrochlore lattice, self-assembly and photonic band gap optimizations. *Opt. Express* 26, 30052–30060 (2018).

32. Gong, Z., Hueckel, T., Yi, G. R. & Sacanna, S. Patchy particles made by colloidal fusion. *Nature* 550, 234–238 (2017).

33. Schade, N. B. et al. Tetrahedral colloidal clusters from random parking of bidisperse spheres. *Phys. Rev. Lett*. 110, 148303 (2013).

34. Wang, Z. et al. Active patchy colloids with shape-tunable dynamics. *J. Am. Chem. Soc*. 141, 14853–14863 (2019).

35. Agard, N. J., Prescher, J. A. & Bertozzi, C. R. A strain-promoted [3 + 2] azide-alkyne cycloaddition for covalent modification of biomolecules in living systems. *J. Am. Chem. Soc*. 126, 15046–15047 (2004).

36. Anderson, J. A., Lorenz, C. D. & Travesset, A. General purpose molecular dynamics simulations fully implemented on graphics processing units. *J. Comput. Phys*. 227, 5342–5359 (2008).

37. Glaser, J. et al. Strong scaling of general-purpose molecular dynamics simulations on GPUs. *Comput. Phys. Commun*. 192, 97–107 (2015).

38. Johnson, S. & Joannopoulos, J. Block-iterative frequency-domain methods for Maxwell's equations in a planewave basis. *Opt. Express* 8, 173–190 (2001).

39. Lee, S., Zheng, C. Y., Bujold, K. E. & Mirkin, C. A. A cross-linking approach to stabilizing stimuli-responsive colloidal crystals engineered with DNA. *J. Am. Chem. Soc*. 141, 11827–11831 (2019).

40. Imhof, A. & Pine, D. J. Ordered macroporous materials by emulsion templating. *Nature* 389, 948–951 (1997). 41. Wijnhoven, J. E. G. J. & Vos, W. L. Preparation of photonic crystals made of air spheres in titania. *Science* 281, 802–804 (1998).

42. Holland, B. T., Blanford, C. F. & Stein, A. Synthesis of macroporous minerals with highly ordered three-dimensional arrays of spheroidal voids. *Science* 281, 538–540 (1998).

43. von Freymann, G. et al. Three-dimensional nanostructures for photonics. *Adv. Funct. Mater*. 20, 1038–1052 (2010).

44. Liu, L., Karuturi, S. K., Su, L. T. & Tok, A. I. Y. TiO2 inverse-opal electrode fabricated by atomic layer deposition for dye-sensitized solar cell applications. *Energy Environ. Sci*. 4, 209–215 (2011).

45. Gratson, G. M. et al. Direct-write assembly of three-dimensional photonic crystals: Conversion of polymer scaffolds to silicon hollow-woodpile structures. *Adv. Mater*. 18, 461–465 (2006).

46. van Blaaderen, A., Ruel, R. & Wiltzius, P. Template-directed colloidal crystallization. *Nature* 385, 321–324 (1997).

47. Leal-Calderon, F., Mondain-Monval, O., Pays, K., Royer, N. & Bibette, J. Water-in-oil emulsions: role of the solvent molecular size on droplet interactions. *Langmuir* 13, 7008–7011 (1997).

48. Chen, Q., Bae, S. C. & Granick, S. Directed self-assembly of a colloidal kagome lattice. *Nature* 469, 381–384 (2011).

49. Bonn, D. et al. Direct observation of colloidal aggregation by critical Casimir forces. *Phys. Rev. Lett*. 103, 156101 (2009).

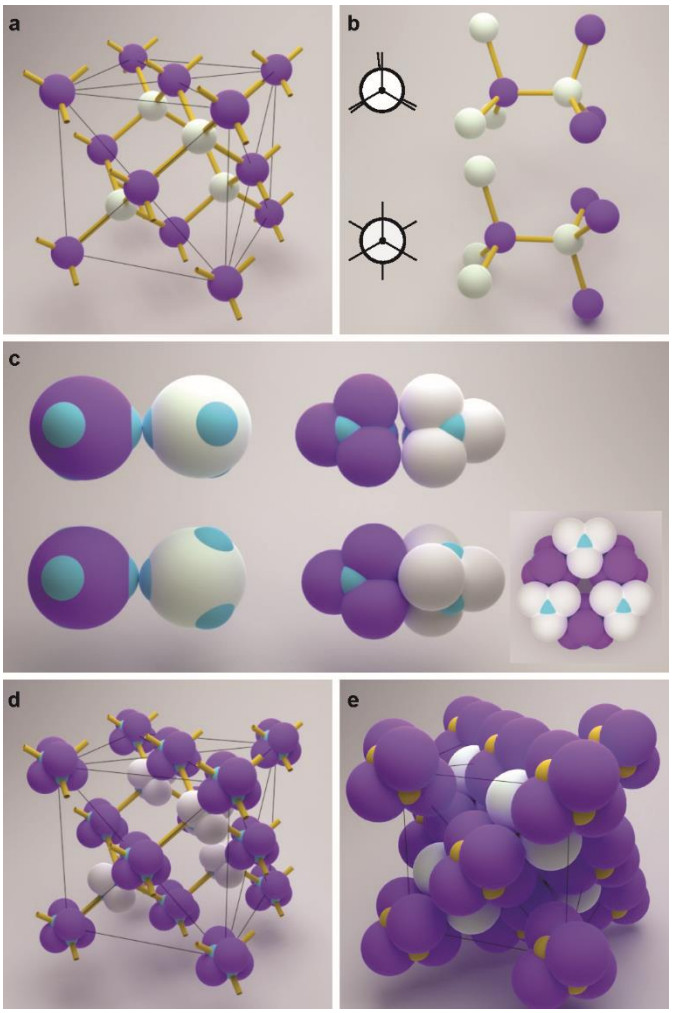

Figure 1: **Schematic and space-filling models of a colloidal diamond lattice. a**, Unit cell of a cubic diamond crystal of spheres: an FCC Bravais lattice with a 2-particle basis (white and purple). Yellow rods show the tetrahedral bonds between atoms. **b**, Top right: eclipsed conformation. Bottom right: staggered conformation. Left: Newman projections. **c**, Left: Bound spherical patchy particles are completely free to rotate about the axis connecting their centers without any preferred orientation. In addition, the finite patch size means that the bond angle is also flexible, making rings of 5, 6, and 7 particles possible. Center: The patches in tetrahedral cluster particles can only reach each other and bind when the spherical lobes interlock, which fixes their patches in the staggered conformation. Right: Bound patchy tetrahedral particles only form six-membered rings, which are in the desired "chair" conformation of cubic diamond, not the "boat" conformation that occurs in hexagonal diamond. **d**, Unit cell of a cubic diamond crystal of patchy clusters, made artificially smaller to make the bonding between patches visible. **e**, Unit cell of a cubic diamond crystal of patchy clusters with correct sizing.

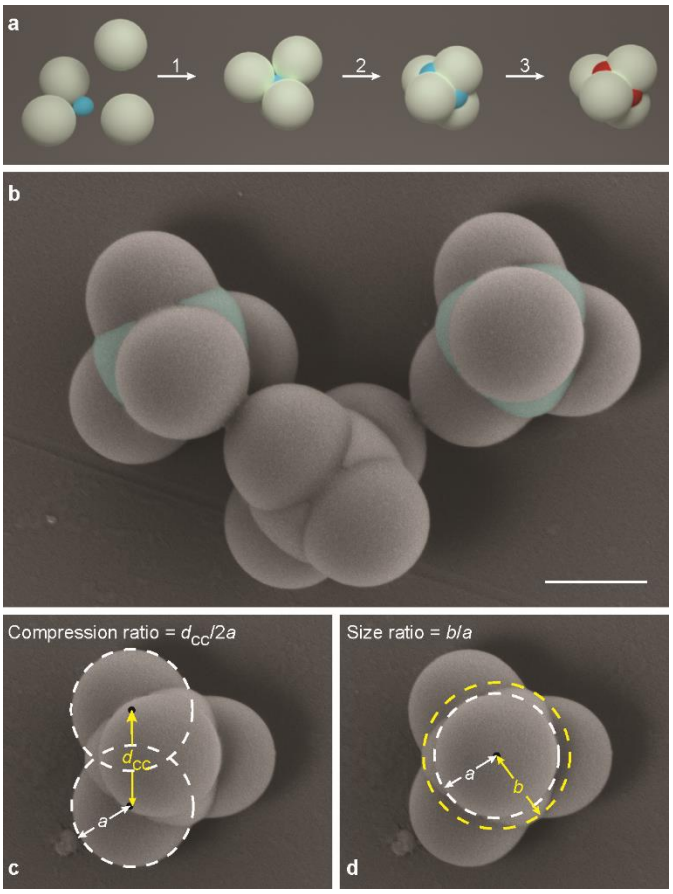

Figure 2: **Synthesis of compressed tetrahedral patchy clusters. a**, (1) Aggregation of four polystyrene (PS) particles (white) around a smaller oil droplet (blue), followed by (2) the controlled deformation of the PS particles with THF, which extrudes the central oil droplet. (3) The THF is then removed, the oil polymerized and coated with DNA to produce solid compressed tetrahedral clusters with DNA-coated patches (red). **b**, SEM image of compressed tetrahedral clusters. Some TPM patches are highlighted in light blue. **c**, The compression ratio dcc=2a is the distance between the centers divided by diameter of the spherical lobes. **d**, The size ratio b=a is the radial extent of the patches from the cluster center divided by the radius of the spherical lobes. For the particles shown here, dcc=2a = 0:78 and b=a = 1:22. Scale bar, 1 _m.

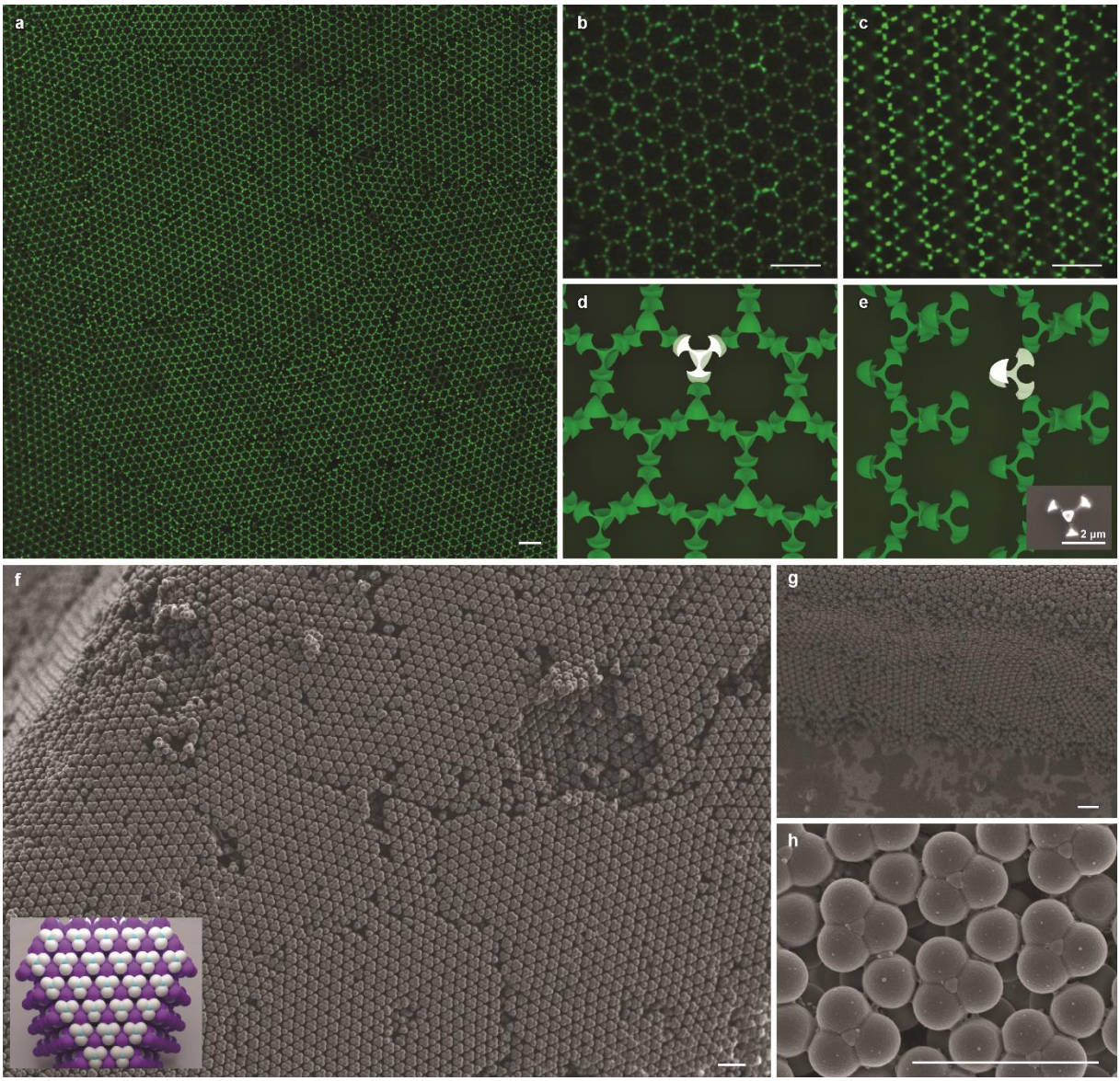

Figure 3: **Crystallization of cubic diamond colloidal crystals. a**, Confocal microscope image showing hexagonal symmetry of the 111 plane characteristic of diamond crystals. The signal originates from the fluorescently-labeled TPM cores of the tetrahedral cluster patchy particles. **b**, Zoomed-in confocal images for the 111 plane and **c**, 110 plane of cubic diamond crystal. **d**, Computer-generated images of the TPM patterns expected for the 111 plane and **e**, 110 plane for cubic diamond crystals. A single TPM core within one compressed cluster is highlighted in white. Inset: scanning electron microscope image of the TPM core, in which polystyrene is dissolved and washed away by THF. **f**, SEM images of the 111 plane of colloidal diamond crystals. Crystal sizes are about 40 _m across with grain boundaries and point defects. Inset: A computer generated image showing 111 plane of colloidal diamond crystal for dcc=2a = 0:74, consistent with the SEM photographs. **g**, Side view of a crystal edge. The thickness of the crystal is about 10 to 20 particles. **h**, Zoomed-in SEM image of the 111 plane showing the interlocking of particles, as designed. For particles shown in **a**, **c**, **f** and **g**, dcc=2a = 0:73 and b=a = 1:20; in **b**, dcc=2a = 0:69 and b=a = 1:18; in **h**, dcc=2a = 0:75 and b=a = 1:19 Scale bar, 5 _m.

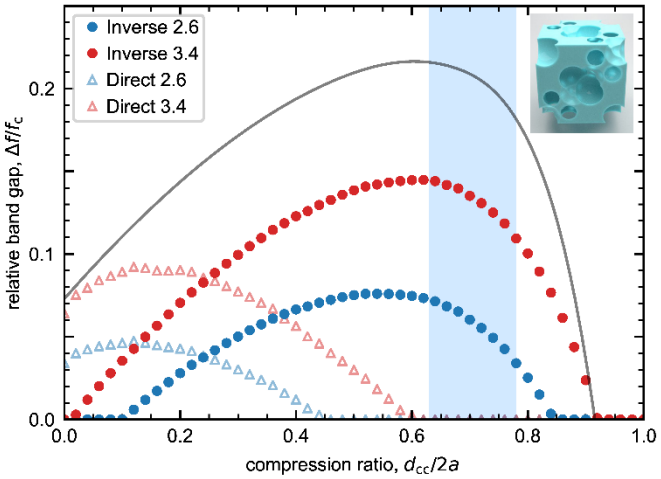

Figure 4: **Relative band gap vs. compression ratio.** Circles and triangles correspond to direct and inverse lattices, respectively. Blue and red points correspond to titania (n = 2:6) and silicon (n = 3:4), respectively. The experimental values for the compression ratio found to crystallize in experiments are highlighted in light blue, showing that the maximum band gap widths for the inverse cluster cubic diamond are realized near the experimental conditions. The gray lines shows the band gap obtained for an inverse silicon lattice where a sacrificial layer of thickness 0:1a is used to coat the colloidal template before backfilling with silicon. Inset: Inverse cubic diamond unit cell with compression ratio of particles in the direct lattice dcc=2a = 0:76.